Regulation of cell attachment, spreading, and migration by hydrogel substrates with independently tunable mesh size

Jing Xia [a, 1], Zong-Yuan Liu [b, 1], Zheng-Yuan Han [a], Yuan Yuan [a], Yue Shao [b], Xi-Qiao Feng [b,*], David A. Weitz [a, c, *]

[a] *School of Engineering and Applied Sciences, Harvard University, Cambridge, MA 02138, USA*

[b] *Institute of Biomechanics and Medical Engineering, Department of Engineering Mechanics, Tsinghua University, Beijing 100084, China*

[c] *Department of Physics, Harvard University, Cambridge, MA 02138, USA*

[1] These authors contribute equally.

* To whom correspondence may be addressed.

Email: fengxq@tsinghua.edu.cn (X.Q.F.), weitz@seas.harvard.edu (D.A.W).

Abstract

Hydrogels are widely used as substrates to investigate interactions between cells and their microenvironment as they mimic many attributes of the extracellular matrix. The stiffness of hydrogels is an important property that is known to regulate cell behavior. Besides stiffness, cells also respond to structural cues such as mesh size. However, since the mesh size of hydrogel is intrinsically coupled to its stiffness, its role in regulating cell behavior has never been independently investigated. Here, we report a hydrogel system whose mesh size and stiffness can be independently controlled. Cell behavior, including spreading, migration, and formation of focal adhesions is significantly altered on hydrogels with different mesh sizes but with the same stiffness. At the transcriptional level, hydrogel mesh size affects cellular mechanotransduction by regulating nuclear translocation of yes-associated protein. These findings demonstrate that the mesh size of a hydrogel plays an important role in cell-substrate interactions.

Statement of Significance

Hydrogels are ideal platforms with which to investigate interactions between cells and their microenvironment as they mimic many physical properties of the extracellular matrix. However, the mesh size of hydrogels is intrinsically coupled to their stiffness, making it challenging to investigate the contribution of mesh size to cell behavior. In this work, we use hydrogel-on-glass substrates with defined thicknesses whose stiffness and mesh size can be independently tuned. We use these substrates to isolate the effects of mesh size on cell behavior, including attachment, spreading, migration, focal adhesion formation and YAP localization in the nucleus. Our results show that mesh size has significant, yet often overlooked, effects, on cell behavior, and contribute to a further understanding of cell-substrate interactions.

Keywords

Cell behavior, Hydrogel substrates, Mesh size, Stiffness, hBMSC, YAP

1. Introduction

Cells interact and respond to their local extracellular microenvironment. It not only serves as an essential physical scaffold for the cells, but it also provides a variety of stimuli that regulate cell behavior [1]. Hydrogels can mimic the attributes of the extracellular microenvironment while allowing control of their mechanical and structural properties [2]; thus they are often used as a material with which to investigate the effects of these properties on cell behavior [3-5]. One of the most important and widely studied physical properties is the stiffness of hydrogel substrate. It is a key mechanical cue that regulates cell behavior and determines stem cell fate [6-9]. However, substrate stiffness cannot be the only parameter controlling cell behavior. Evidence has emerged that structural cues are of essential importance in guiding cell response [10, 11]. For example, the decrease of the hydrogel mesh size can induce significant osteogenic differentiation of human stem cells [12]. However, contradictory results have reported that osteogenic and adipogenic differentiation of human stem cell is not affected by varying the mesh size of hydrogel [13]. This debate arises from the fact that the mesh size of the hydrogel is intrinsically coupled with the stiffness [14-17], making it very difficult to investigate the independent contribution of hydrogel mesh size to cell behavior. Furthermore, most studies have focused only on longer-term response such as cell differentiation, which happens over weeks, while how the mesh size affects shorter-term responses, such as attachment, spreading, and migration, which happen over hours to a few days, have been overlooked. To distinguish the contribution of mesh size, it is of critical importance to decouple the effects of mesh size and stiffness; this will enable investigation of the corresponding cell behavior such as attachment, spreading, and migration.

In this study, we report a hydrogel system whose stiffness and mesh size can be independently controlled, thereby, enabling us to isolate the effect of mesh size on the behavior of human bone marrow-derived mesenchymal stem cells (hBMSCs). By attaching the hydrogel with a defined thickness to the surface of a solid glass slide, we fabricate a hydrogel-on-glass substrate. The stiffness of this composite substrate is determined by a combination of the thickness and mesh size of the hydrogel layer; thus, by varying the thickness and the monomer concentration, the stiffness and mesh size of the hydrogel-glass substrate can be adjusted independently. We then grow cells on these substrates with the same stiffness but different mesh sizes, and investigate their behavior, including attachment, spreading, and migration. We find that the attachment of cells is not sensitive to the changes in hydrogel mesh size. By contrast, as the mesh size of hydrogel decreases, cells have significantly larger spreading areas and nuclear projected areas. Furthermore, cells migrate much faster on hydrogels with smaller mesh sizes. At the subcellular scale, cells form bigger focal adhesions on the hydrogels with smaller mesh sizes, indicating better adhesion between cells and hydrogels. Furthermore, we show that more yes-associated protein (YAP) translocates from the cytoplasm to the nucleus in the cells grown on the hydrogels with smaller meshes, indicating a regulatory role of hydrogel mesh size in the cellular mechanotransduction. These results demonstrate that the mesh size of hydrogel has significant effects on cell behavior and plays an important role in the cell-substrate interaction.

2. Materials and Methods

2.1. Fabrication of hydrogel-on-glass substrates with defined thicknesses

Glass slides are functionalized using (3-Aminopropyl)triethoxysilane (APTES; Sigma-Aldrich, MO, USA) to facilitate covalent attachment of the hydrogel to glass. Briefly, glass slides are cleaned for 60 seconds using plasma cleaner (Diener electronic GmbH + Co. KG, Germany) at the power of 100 mW. The glass slides are then immersed in ethanol (Sigma-Aldrich, MO, USA) containing 1% APTES and 1% 1 M NaOH (Sigma-Aldrich, MO, USA) for 10 min. The glass slides are subsequently washed with ethanol twice and rinsed with deionized water. The glass slides are left at room temperature until completely dried.

A prepolymer solution is prepared with a total volume of 1124 µL containing acrylamide monomers (Sigma-Aldrich, MO, USA), *N, N′*-Methylene-bisacrylamide (Sigma-Aldrich, MO, USA), 15 µL of 10% weight percentage ammonium persulfate (Sigma-Aldrich, MO, USA), 0.5 µL *N, N, N′, N′*- tetramethylethylenediamine (Sigma-Aldrich, MO, USA) and beads of different diameters in deionized water. To tune the mesh size of the hydrogel, acrylamide monomer and *N,N′*-Methylenebisacrylamide are prepared at final weight percentages of 6% / 0.35%, 9% / 0.126%, and 12% / 0.065% in the prepolymer solution. To adjust the thickness of the hydrogel (2.5 µm, 15 µm, 30 µm, and 200 µm), beads of different diameters are added to the prepolymer solution, which are 2.5 µm (Magsphere, CA, USA), 15 µm (Bangslab, Indiana, USA), 30 µm (Sigma-Aldrich, MO, USA), and 200 µm (Sigma-Aldrich, MO, USA). The density of the beads is controlled such that the distance between the beads is at least 300 µm. To fabricate thick hydrogels (1000 µm), we add plastic spacers of 1000 µm at the edge of the coverslip. The prepolymer solution is then transferred to the pre-treated glass slides and then covered with 18-mm diameter coverslips. Two magnets, one on the top of the coverslip, one beneath the bottom of the glass slide, are used to press the coverslip and slide. After 3 hours, the coverslip is gently peeled off and hydrogels are immersed in phosphate-buffered saline solution (Sigma-Aldrich, MO, USA).

2.2. DNA gel electrophoresis

Ultra-Low Range DNA Ladder (Thermo Scientific, MA, USA) is mixed with TriTrack DNA Loading Dye (contains Xylene Cyanol FF, Bromophenol Blue, and Orange G) (Thermo Scientific, MA, USA) and run through polyacrylamide electrophoresis hydrogels in TAE buffer at 110V for 30 minutes. The samples are stained with GelRed Nucleic Acid Stain (Sigma-Aldrich, MO, USA) and imaged with a homemade imaging system built with a camera, a PC, and a UV/white light dual-light source.

2.3. Measurement of the Young's modulus of hydrogels

Polyacrylamide hydrogels are polymerized into cylindrical-disk shapes with 35-mm diameter and 10-mm thickness using petri dishes as molds. The hydrogel samples are immersed in PBS for at least 3 hours such that the swelling of the hydrogel can reach its equilibrium. Nanoindentation measurements are performed using a nanoindenter (Agilent G200, Agilent Technologies, Santa Clara, USA) with a 100-µm-diameter cylindrical diamond probe. For each composition of hydrogels, two samples are prepared and six individual measurements are performed on each sample at different locations, with at least a 200-µm distance between two neighboring locations. Young's modulus is obtained from the continuous stiffness measurement (CSM) mode of the instrument at an amplitude of 500 nm and a frequency of 10 Hz.

135

136 *2.4. Atomic force microscopy*

137 The stiffness of the hydrogel-on-glass substrate with defined thickness is measured with
138 an atomic force microscope (Nanowizard; JPK, Berlin, Germany). Silicon nitride
139 cantilevers with spherical tips of 3.5-µm diameter (NanoAndMore USA Corporation, CA,
140 USA) are used. The hydrogel samples are immersed in PBS for at least 3 hours such
141 that their swelling can reach equilibrium. Samples are indented at 9 positions with a
142 distance of at least 17 µm apart between two neighboring positions. Samples are
143 indented at an approach velocity of 5 µm/s until a 2 nN trigger force is registered, and
144 the tip is then retracted at 5 µm/s. The linear portion of the indentation force–depth curve
145 is analyzed with the JPK data processing software to extract the stiffness of the sample
146 by fitting the indentation curve with the Hertzian model.

147

148 *2.5. Functionalization of the substrate with collagen*

149 These substrates are coated with collagen such that the cells can attach to the substrate
150 well. Briefly, the samples are immersed in Hepes buffer (pH 8.5, Sigma-Aldrich, MO,
151 USA) and then sterilized under germicidal light in a cell culture hood for 20 mins. Then
152 the samples are immersed in 0.125 mg/ml N-sulphosuccinimidyl-6-(4'-azido-2'-
153 nitrophenylamino) hexanoate (sulfo-SANPAH; Thermo Scientific, MA, USA), activated
154 with 365-nm UV light (Analytik Jena, Germany), washed, and then incubated overnight
155 in 200 µg/ml rat type-I collagen solution (Sigma-Aldrich, MO, USA).

156

157 *2.6. Immunofluorescence staining of collagen*

158 Substrates with collagen coating are blocked with 1% bovine serum albumin (Sigma, MO,
159 USA) in PBS for 1 hour, followed by a two-step immunostaining process. Briefly,
160 samples are first incubated with mouse monoclonal anti-collagen I antibodies (ab90395,
161 Abcam, MA, USA) diluted 200X in PBS with a supplement of 1% bovine serum albumin
162 for 1 hour at room temperature. Samples are then washed 5 times with PBS and
163 incubated with goat anti-mouse Alexa fluor plus 488 secondary antibodies (Thermo
164 Fisher Scientific Inc, MA, USA) diluted 200X in PBS with a supplement of 1% bovine
165 serum albumin for 1 hour in the dark. Samples are washed 3 times with PBS before
166 imaging. Substrate without collagen coating is stained with the same protocol as a
167 negative control. The stained samples are then fluorescently imaged with a confocal
168 microscope equipped with a 25X/0.95-NA water immersion objective (TCS-SP5; Leica
169 Microsystems Inc., IL, USA).

170

171 *2.7. Collagen quantification with enzymatic assay*

172 To compare the collagen amount on the surface of the hydrogel, the ELISA kit (Chondrex,
173 Inc. WA, USA) is partially adapted and the relative amount of collagen is determined
174 based on changes in the optical density. Briefly, the samples are blocked with 1% BSA in
175 PBS. The samples are then incubated with Peroxidase-Conjugated Goat Anti-Rat
176 antibody at room temperature for 1 hour. The samples are subsequently washed 3 times
177 and incubated with TMB solution for 15 minutes. The stop solution is added to each
178 sample and the optical density of the reacted solution is read at 450 nm.

179

180 *2.8. Scanning electron microscopy*

181 For observation of the hydrogel microstructure with a scanning electron microscope,
182 fixed samples are dehydrated in ethanol graded series (50%, 60%, 70%, 80%, 90%,
183 100%, Sigma, MO, USA) for 30 minutes each and eventually immersed in 100% ethanol
184 for 2 hours. After dehydration, samples are transferred to a critical point dryer (Tousimis
185 931GL, MD, USA) and dried under the critical point of CO_2. Samples are then coated
186 with 5 nm Pt/PD and observed with an Ultra 55 scanning electron microscope (Carl
187 Zeiss Microscopy, LLC, NY, USA).
188

189 *2.9. Cell culture*

190 Human bone marrow-derived mesenchymal stem cells (hBMSCs; ATCC, VA, USA) are
191 used in this study. MSC growth medium is prepared by mixing mesenchymal stem cell
192 basal medium (ATCC, VA, USA) with mesenchymal stem cell growth kit (ATCC, VA,
193 USA). Cells are cultured in the MSC growth medium and maintained in the 37 °C, 5%
194 CO_2 infused incubator. All experiments are carried out with early passage hBMSCs
195 (passage 2–passage 6).

196

197 *2.10. Cell attachment and migration assay*

198 Cells are seeded onto substrates at a density of ~4000 cells/cm^2 and cultured in MSC
199 growth medium. Nuclei of cells are stained with 0.5 μM SiR-DNA staining reagents
200 (Cytoskeleton Inc., DENVER, CO, USA). To perform the live-cell imaging, substrates
201 with cells are kept in an incubator (OKO lab, NA, Italy) supplemented with 5% CO_2 and
202 maintained at 37 °C. The cells are imaged for continuous 4 days with a confocal
203 microscope equipped with a 10X/0.3-NA dry objective (TCS-SP5; Leica Microsystems
204 Inc., IL, USA).

205

206 *2.11. Cell morphology assay*

207 To observe the morphology of cells, cells are seeded on substrates at a density of ~4000
208 cells/cm^2. We fluorescently stain the cell cytoplasm with 2 μg/ml CellTracker™ green
209 (Thermo Fisher Scientific Inc, MA, USA) and stain the cell nucleus with 0.5 μM SiR-DNA
210 (Cytoskeleton Inc., DENVER, CO, USA). The stained cells are fixed with 4%
211 formaldehyde and imaged with a confocal microscope equipped with a 25X/0.95-NA
212 water immersion objective (TCS-SP5; Leica Microsystems Inc., IL, USA).

213

214 *2.12. Immunofluorescence assay of focal adhesion*

215 Cells are seeded on substrates at a density of ~4000 cells/cm^2 and cultured in an
216 incubator infused with 5% CO_2 and maintained at 37 °C. After 16 hours, cells are fixed
217 with 4% formaldehyde and 0.1% Triton X100 diluted in PBS, followed by PBS wash 3
218 times to remove excessive reagents. Fixed cells are then triple stained for actin, vinculin,
219 and nucleus: fixed cells are blocked with 10% normal goat serum (Thermo Fisher
220 Scientific Inc, MA, USA) in PBS for 1 hour, followed by a two-step immunostaining
221 process for vinculin. Briefly, cells are first incubated with mouse monoclonal anti-vinculin

antibodies (Sigma-Aldrich, MO, USA) diluted 200X in PBS with a supplement of 10% normal goat serum for 1 hour at room temperature. Samples are then washed 5 times with PBS and incubated with goat anti-mouse Alexa fluor plus 488 secondary antibodies (Thermo Fisher Scientific Inc, MA, USA) diluted 200X in PBS with a supplement of 10% normal goat serum for 1 hour in the dark. Phalloidin-iFluor 555 (Abcam, MA, USA) and Draq 5 nucleus probe (Thermo Fisher Scientific Inc, MA, USA) are diluted at ratios of 1:1000 and 1:5000 each to stain actin and nuclei of cells. Stained cells are washed 3 times with PBS and imaged with a confocal microscope equipped with a 63X/1.20-NA water immersion objective (TCS-SP5; Leica Microsystems Inc., IL, USA).

2.13. Immunofluorescence assay of YAP

Cells are seeded on substrates at a density of ~4000 cells/cm^2 and cultured in an incubator infused with 5% CO_2 and maintained at 37 ^oC. After 16 hours, cells are fixed with 4% formaldehyde and 0.1% Triton 100X diluted in PBS, followed by PBS wash 3 times to remove excessive reagents. Fixed cells are triple stained for actin, YAP, and nucleus: fixed cells are blocked with 10% normal goat serum (Thermo Fisher Scientific Inc, MA, USA) in PBS for 1 hour, followed by a two-step immunostaining process for YAP. Briefly, cells are incubated with rabbit polyclonal anti-YAP antibodies (Cell Signaling Technology, Inc., MA, USA) diluted 200X in PBS with a supplement of 10% normal goat serum for 1 hour at room temperature. Samples are then washed 5 times with PBS and incubated with goat anti-rabbit Alexa fluor plus 594 secondary antibodies (Thermo Fisher Scientific Inc, MA, USA) diluted 200X in PBS with a supplement of 10% normal goat serum for 1 hour in the dark. Phalloidin-iFluor 555 (Abcam, MA, USA) and Draq 5 nucleus probe (Thermo Fisher Scientific Inc, MA, USA) are diluted at ratios of 1:1000 and 1:5000 each to stain actin and nuclei of cells. Stained cells are washed 3 times with PBS and imaged with a confocal microscope equipped with a 63X/1.2-NA oil immersion objective (LSM880; Nikon Instruments Inc. NY, USA).

2.14. Image analysis

To quantify the collagen coating on substrates, the fluorescence intensity of the confocal images is measured with Image J (https://imagej.nih.gov/ij/). For the cell attachment study, the number of the cell nucleus is counted with the particle analyzer plugin in Image J. For the cell morphology study, fluorescence images of cells are segmented by OTSU's method; cell spreading area and nuclear projected area are further measured with particle analyzer plugin in Image J. For the cell migration study, fluorescent images of the cell nucleus are contiguously recorded with a 5-minute interval. The migration trajectories of cells are extracted by tracking their nuclei with the particle tracker plugin in Image J. The extracted trajectories are then analyzed with MATLAB (Mathworks, MA, USA) to calculate cell migration speed and directional persistence. Analysis of focal adhesions is performed according to a previous method [18]. For the YAP nuclear translocation study, the total fluorescence intensity of YAP in the nuclear and cytoplasmic regime are quantified with Image J.

2.15. Statistical analysis

Statistical analysis is performed using Origin software (OriginLab Corporation, MA, USA). The one-way analysis of variance (ANOVA) is used to determine whether there are any statistically significant differences between multiple comparisons [19]. P-values larger than 0.05 are assumed to be non-significant in all analyses; P-values smaller than 0.05 are assumed to be significant and marked with *; P-values smaller than 0.01 are marked with **; P-values smaller than 0.001 are marked with ***; P-values smaller than 0.0001 are marked with ****.

3. Results and Discussion

3.1. Preparation of hydrogel substrates with different mesh sizes but the same stiffness

To decouple the stiffness of the hydrogel from its mesh size, we fabricate a composite substrate where a hydrogel of controlled thickness is cast on the surface of a rigid, glass slide. The stiffness of this composite substrate is determined by both the intrinsic stiffness of the hydrogel, which depends on its mesh size, and the thickness of the hydrogel layer. Then, by adjusting both the intrinsic stiffness of the hydrogel and its thickness, we can independently control the mesh size and stiffness of the composite substrate. We fabricate these composite substrates by casting polyacrylamide (PAA) hydrogel layers onto glass slides treated with 3-Aminopropyltriethoxysilane (APTES). The treatment of APTES on the glass slides enables strong covalent binding of the polyacrylamide (PAA) hydrogel to the glass slides. To ensure cells adhere to the hydrogels, we covalently couple type-I collagen molecules to the hydrogel surface using the heterobifunctional linker sulfosuccinimidyl 6-(4'-azido-2'-nitrophenylamino) hexanoate (sulfo-SANPAH), as shown in Figure 1(a).

To change the mesh size of the hydrogel, we tune the concentrations of acrylamide monomer and crosslinker *N,N'*-Methylene-bisacrylamide, which are used for PAA hydrogel polymerization. We make three samples: the first sample has a weight/volume percentage concentration of 6% monomer and 0.35% crosslinker; the other two samples have monomer/crosslinker weight/volume percentage concentrations of 9%/0.126%, and 12%/0.065%, respectively. To compare the mesh size of hydrogels, we freeze dry samples and observe them with scanning electron microscopy (SEM). The mesh size of the dried hydrogel decreases as the acrylamide concentration increases, as shown in Figure 1(b). However, the value measured with SEM is likely an overestimation of the mesh size of the hydrogel in its hydrated state due to structural collapse during the sample drying process [12, 13]. To qualitatively compare the mesh size among hydrogel samples, we measure the dynamics of DNA fragments passing through the hydrogels in their hydrated state by gel electrophoresis. The mobility of the DNA fragment is an indicator of the relative mesh size among hydrogel samples; higher mobility of the DNA fragment indicates a larger mesh size [20-22]. We fabricate the hydrogels following the same protocol as those for SEM imaging but without drying them. We find that DNA fragments migrate faster in hydrogels with lower concentrations of acrylamide, as shown in Figure 1(c). In addition, the same observation has been made on the mobility of DNA loading dyes, as shown in Figure S1. This suggests that hydrogels with lower concentrations of acrylamide have larger mesh sizes; the relative size of hydrogel mesh is also consistent with those measured with SEM. Taken together, all three measurements are consistent and confirm that the mesh size of the hydrogel decreases as the acrylamide concentration increases from 6% to 12%.

The variation of hydrogel mesh size with composition also leads to a variation in the

intrinsic stiffness of the hydrogel. To determine the intrinsic stiffness of the hydrogel, we fabricate a thick layer (~10mm) of the polyacrylamide hydrogel and measure its intrinsic stiffness with a nanoindenter. As the acrylamide concentration increases from 6% to 12%, the intrinsic stiffness, or Young's modulus of the hydrogel, decreases from ~15 kPa to ~7.5 kPa, as shown in Figure S2. To adjust the stiffness of the composite substrates, we fabricate hydrogel layers with different thicknesses onto the glass slides [23-25]. We use two different methods to vary the thickness of PAA hydrogel layers, either by adding spacer beads with a certain diameter [24] or by adding plastic spacers, as shown in Figure 1a. For the spacer beads, we intentionally control the density of the beads in the hydrogels such that the distance between the beads is at least 300 μm, which is much larger than the size of a single cell (~80 μm). Therefore, when the cells are cultured on substrates, most of them do not contact beads and are not influenced by the beads. The stiffness of the hydrogel-glass substrate is measured with atomic force microscopy (AFM). A typical indentation force–depth curve of AFM measurement is shown in Figure S3. For each of the different compositions, the stiffness decreases rapidly as the thickness increases, but saturates at the intrinsic stiffness of the hydrogel when the thickness is greater than 30 μm, as shown in Figure S4. To select the substrates with the same stiffness, we choose the overlapping stiffness range of hydrogel substrates with different mesh sizes, which is ~12-15kPa. Therefore, we select three substrates with the same stiffness of ~13kPa: 30-μm thick PAA at an acrylamide concentration of 6%, 15-μm thick PAA at 9%, and 2.5-μm thick PAA at 12%. The stiffnesses of these three samples are very nearly the same, as shown in Figure 1(d). Nevertheless, the mesh sizes are clearly distinct, as evidenced from Figures 1(b) and (c). For simplicity, these three substrates are referred to as PAA 6%, PAA 9%, and PAA 12%, respectively. In this manner, hydrogel mesh size is the only changing parameter and its effect on the cell behavior can be decoupled from the hydrogel stiffness.

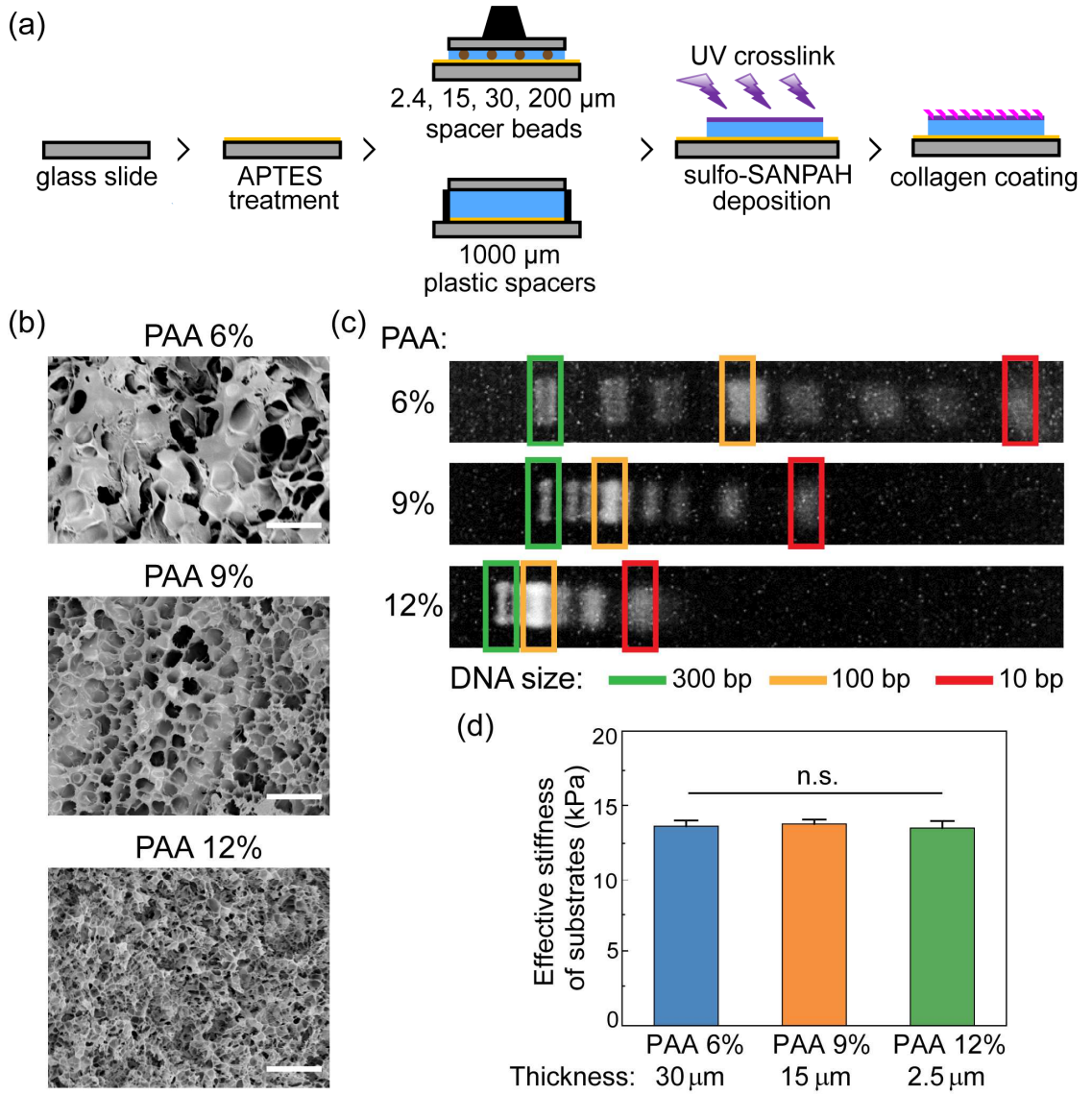

Figure 1. Fabrication of hydrogel-on-glass substrates with different mesh sizes but the same stiffness. (a) Schematic of the fabrication workflow of hydrogel-on-glass substrates with defined thicknesss. (b) Representative SEM images of PAA hydrogels with different acrylamide concentrations. Scale bars, 5 μm. (c) Electrophoresis of DNA fragments in hydrated PAA hydrogels with different acrylamide concentrations. (d) Stiffness of the hydrogel-on-glass substrates with indicated acrylamide concentrations and hydrogel thicknesses (Mean ± SD, *N*=9 per group, one-way ANOVA, P>0.05).

3.2. Characterization of collagen coating on hydrogels with different mesh sizes

Cells do not readily attach to PAA hydrogels due to the lack of anchoring sites [26]; therefore, extracellular matrix (ECM) ligands, such as collagen, must be bound to the surface of the hydrogel to provide the essential anchoring sites for cells [27, 28]. In this study, we coat the hydrogels with sulfo-SANPAH, a protein crosslinker, and then covalently link collagen molecules to the sulfo-SANPAH. The same concentration of sulfo-SANPAH and collagen are used for all the hydrogels.

To ensure that any observed differences in cell behavior do not originate from the ECM protein functionalization, the collagen coating of the hydrogels is interrogated using three methods: a direct fluorescence quantification assay, an immunostaining assay and an enzymatic assay. To perform the direct fluorescence quantification assay, we coat the hydrogel surface with a mixture of FITC-labeled and unlabeled collagen at a ratio of 5:1, and quantify the surface fluorescence with confocal microscopy according to a previously reported method [29-31]. We find that spot-like collagen is randomly distributed on all hydrogel surfaces, as shown in Figure 2(a). This is in contrast to the rod-like fibers of collagen assembled under the physiological condition [32, 33]. We attribute this difference to the deposition of sulfo-SANPAH on the PAA hydrogel surface, which disrupts fiber formation of collagen monomers due to the non-specific protein conjugation and the blockage of triple helixes [34-36]. We then quantify the average fluorescence intensity of the collagen coatings among different samples. The fluorescence intensity of the collagen coating is nearly the same among samples with no obvious difference, as shown in Figure 2(b). This conforms with the previous finding that the collagen coating does not change as the hydrogel structure changes [37, 38]. To further confirm this result, we performed the second assay, an immunostaining assay. We coat the hydrogel surface with unlabeled collagen and immunofluorescence stain them, as shown in Figure S5(a). We observe similar collagen structures and averaged fluorescence intensity among the collagen coating of hydrogels, as shown in Figure S5(b). In the absence of any collagen coating, the measured fluorescence intensity is one order of magnitude smaller, confirming that the fluorescence measured is from the collagen coating, as shown in Figure S6. To verify that the amount of the collagen coating quantified by the confocal imaging method is not biased by the resolution of the imaging technique, we quantify the collagen coating of hydrogels with an enzymatic assay as the third method. Briefly, collagen coatings are incubated with peroxidase-conjugated collagen antibodies to allow them to bind; the amount of bound peroxidase-conjugated antibodies is proportional to the amount of collagen coating. We then add 3,3',5,5'-Tetramethylbenzidine (TMB) substrate to the samples and allow it to react with the peroxidase-conjugated collagen antibodies to produce a measurable color change, as depicted in Figure 2(c). The optical density of the reaction product at 450 nm is used as an indicator of the collagen coating amount. The optical density values show no observable difference among different hydrogels, as shown in Figure 2(d). Therefore, we conclude that there is no difference in collagen coatings across hydrogels with different mesh sizes.

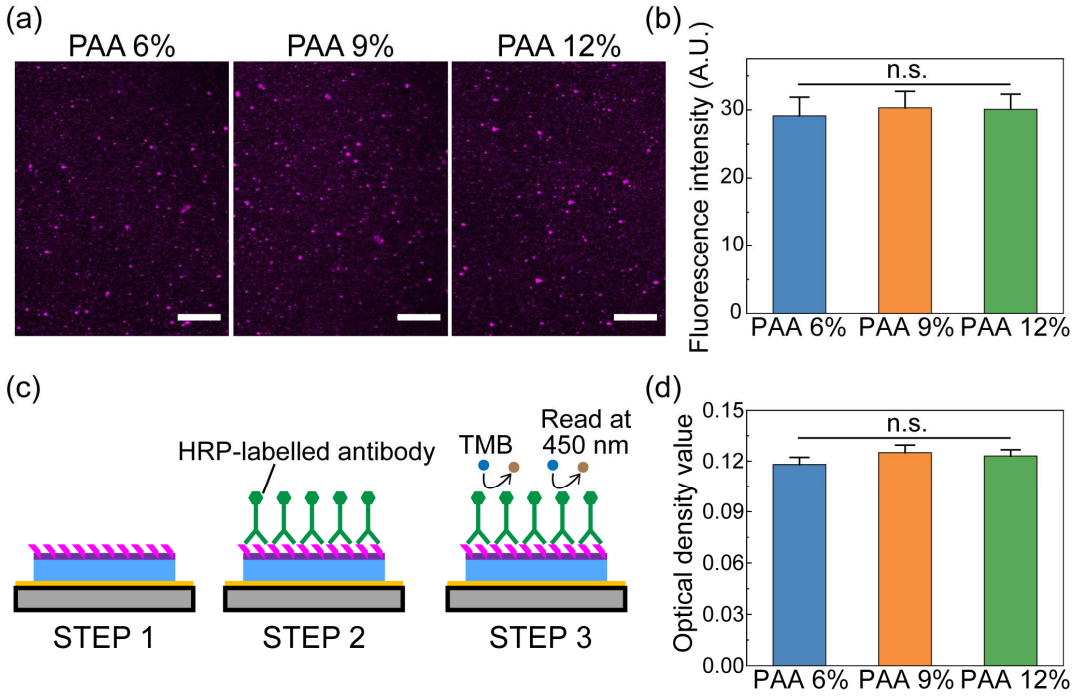

Figure 2. Characterization of collagen coating on hydrogels. (a) Representative fluorescence images of FITC-labeled collagen on different hydrogels. Scale bars, 50 μm. (b) The average fluorescence intensity of FITC-labeled collagen on different hydrogels (Mean ± SD, *N*=20 per group, one-way ANOVA, p>0.05). (c) Schematic of the enzymatic detection assay of collagen coating on hydrogels. (d) Optical density values of peroxidase-TMB reaction product measured on different hydrogels (Mean ± SD, *N*=9 per group, one-way ANOVA, p>0.05).

3.3. Effects of hydrogel mesh size on the cell attachment

To investigate how cells respond to hydrogels with different mesh sizes, we culture cells on these different substrates and observe their corresponding behavior. The first behavior we investigate is the cell attachment, which is the initial step in the cascade of cell-substrate interactions. Cells are seeded onto hydrogels at a low density of ~4000 cells/cm^2, so that most cells are isolated, without cell-cell contact. Cells are well separated on different substrates, as shown by the representative confocal images in Figure 3(a). The number of attached cells is quantified and normalized by the total cell number seeded in the medium to calculate the percentage of cells that are successfully attached to the substrates. For the conditions used in all experiments, at least 80% percent of the cells attach to the hydrogels, and no statistically significant difference in cell-attachment percentage is found among the different substrates, as shown in Figure 3(b). We therefore conclude that the influence of the mesh size of the hydrogel on cell attachment is negligible. A possible interpretation of this observation is that the cell attachment is predominantly determined by the collagen coating on the hydrogel surface [39], for which we observe no differences under our experimental conditions.

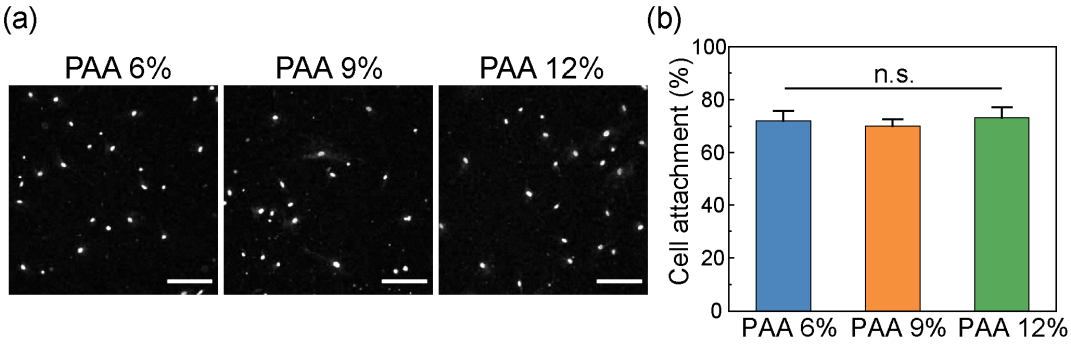

Figure 3. Attachment of cells on hydrogels with different mesh sizes. (a) Representative confocal fluorescence microscopy images of cells on different hydrogels with nuclei stained; cells are imaged 12 h after they are seeded. Scale bars, 200 μm. (b) Percentage cells attached on different hydrogels (Mean ± SE, *N*=26 per group, one-way ANOVA, p>0.05).

3.4. Effect of hydrogel mesh size on the cell morphology

Shortly after their initial attachment, cells will stretch themselves and spread on the substrates. The morphology of the cell has important consequences on cell metabolism [40], as it can determine whether or not a cell proliferates [41], or dies [42]. We investigate the morphology of the fully spread cells on different substrates. We seed cells on the substrates at a low density of ~4000 cells/cm^2. We fluorescently stain the cells with CellTracker™ green to determine their spreading area. We also fluorescently stain the nuclei with DNA dye DRAQ5 to determine their nuclear projected area; representative images obtained with confocal microscopy are shown in Figure 4(a). Cell spreading area and nuclear projected area are quantified from the confocal microscopy images using Image J software. The results suggest that the cell spreading area is significantly larger on hydrogels with smaller mesh sizes, as shown in Figure 4(b). However, the circularity of cells, defined as $4\pi \times Area/Perimeter^2$, exhibts no difference on hydrogels with different mesh sizes, as shown in Figure S7. Moreover, the nuclear projected area follows the same trend as the cell spreading area, as shown in Figure 4(c). Our results demonstrate that by varying the mesh size of the hydrogel, the spreading behavior of cells is pronouncedly altered. Interestingly, the same correlation between cell spreading and nuclear projected area is also reported for cells grown on substrates with different stiffnesses and microstructures [43-45], possibly indicating a similar regulating mechanism of hydrogel mesh size that determines the cell spreading and nuclear projected area.

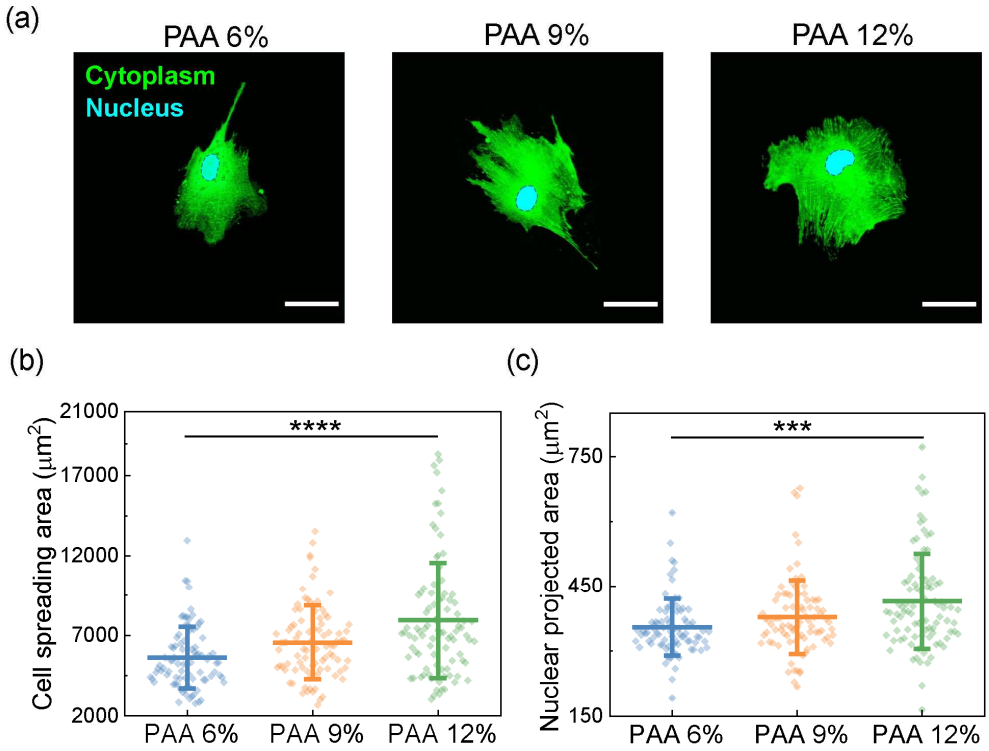

Figure 4. Morphology of cells on hydrogels with different mesh sizes. (a) Representative confocal microscopy images of cells on different hydrogels. The cytoplasm of the cell is depicted in green; the nucleus of the cell is depicted in cyan. Scale bars, 50 μm. (b) Cell spreading area on different hydrogels (Mean ± SD, *N*>88 per group, one-way ANOVA, p<0.0001). (c) Nuclear projected area on different hydrogels (Mean ± SD, *N*>88 per group, one-way ANOVA, p<0.0001).

3.5. Effect of hydrogel mesh size on the cell migration

Besides cell spreading, mechanical and structural cues also influence a series of other cell functions, in particular, cell migration, which is closely associated with cell attachment and spreading [46]. Cell migration is the dynamic movements of cells that is essential for morphogenesis and tissue remodeling [47, 48]. To investigate cell migration on the hydrogels, cells are seeded sparsely enough to avoid cell-cell interactions and are imaged with confocal microscopy over 48 hours. Trajectories of cell migration are extracted from the confocal images with Image J software. Cells migrate in a random pattern without any directional preference and do so on hydrogels with different mesh sizes, as shown by the overlays of cell migration trajectories in Figure 5(a). Our finding is in stark contrast with the directed motion of cells on fibrous collagen networks that results from the strong contact guidance of collagen fibers [49-51], suggesting that the random migratory behavior observed here likely results from the non-fiber structure of the collagen coating.

We then determine the efficiency of the cell migration, which depends on two essential parameters: migration speed, which is how fast a cell moves, and directional persistence, which is how robustly a cell moves along the same direction. We first calculate the average migration speed of the cells, which is determined by dividing the contour length

of the migration trajectory by its duration. We find that cells migrate faster on hydrogels with smaller meshes, as shown in Figure 5(b). Additionally, we determine the distribution of the average migration speeds among cells; for all hydrogels, the distribution is broad and there is a slight shift in the shape, with more faster cells as the mesh size decreases, as shown in Figure 5(c). The other determining parameter of the cell migration efficiency is the directional persistence, which is a parameter that quantifies the straightness of the trajectory and is determined by the ratio of the end-to-end distance to the contour length of each trajectory [52, 53]. In contrast to the average migration speed, the directional persistence exhibits no difference among hydrogels with different mesh sizes, as shown in Figures 5(d) and (e). These results suggest that cell migration efficiency is improved on hydrogels with smaller mesh sizes, which is caused by the increased migration speed, even though there is no change in directional persistence.

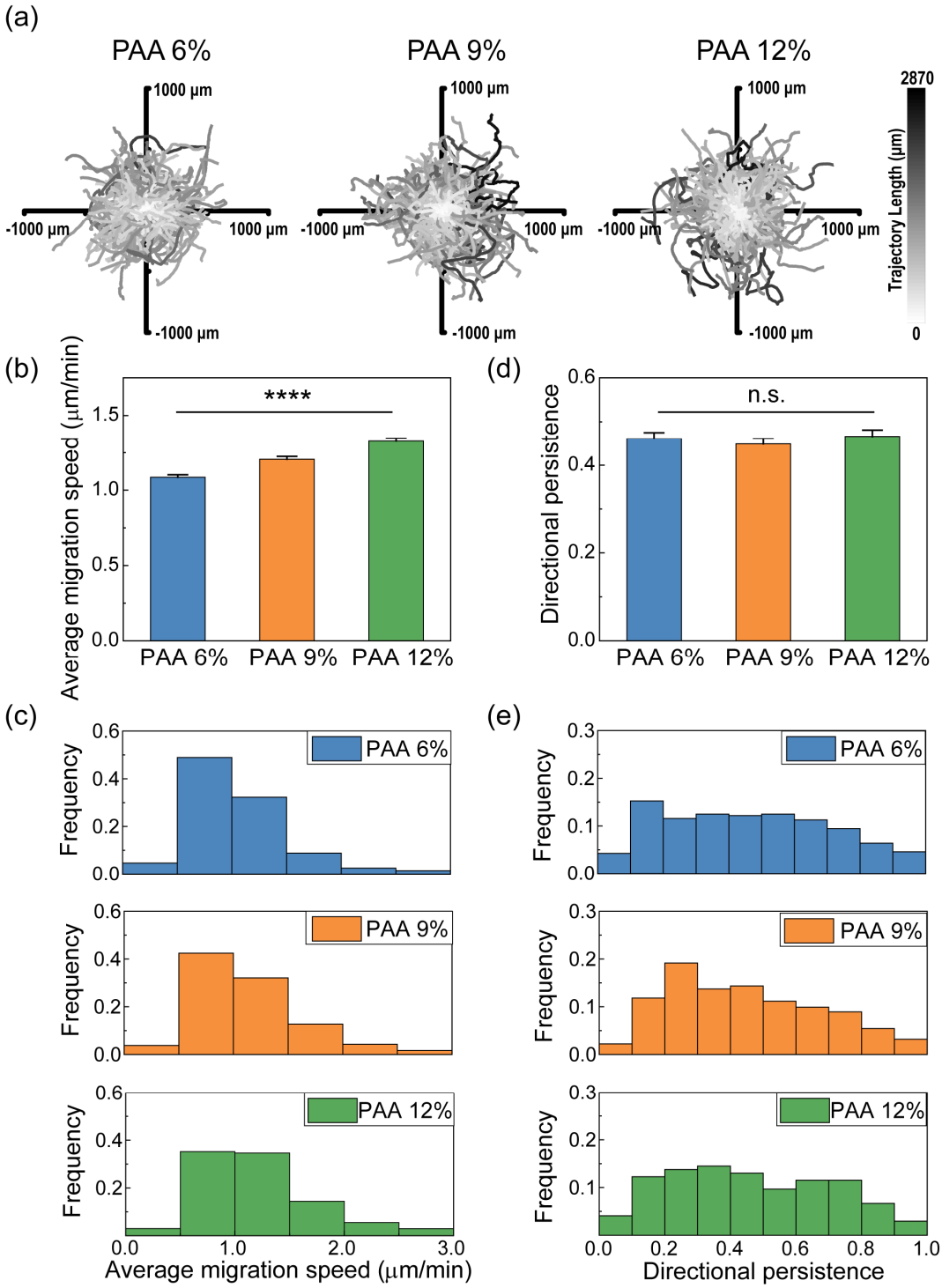

Figure 5. Migration behavior of cells on hydrogels with different mesh sizes. (a) Migration trajectories of cells on different hydrogels (*N*>269 per group). (b) Average migration speed of cells on different hydrogels (Mean ± SE, *N*>269 per group, one-way ANOVA, p<0.0001). (c) Distribution of average migration speed of cells on different hydrogels (*N*>269 per group). (d) Directional persistence of cells on different hydrogels (Mean ± SE, *N*>269 per group, one-way

ANOVA, $p>0.05$). (e) Distribution of directional persistence of cells on different hydrogels ($N>269$ per group).

3.6. Effect of hydrogel mesh size on the formation of focal adhesions

Given the dramatic changes in the spreading and migration behavior of cells with different hydrogel mesh sizes, we hypothesize that there is a corresponding change in the focal adhesion, which is a key mechanosensor at the interface between the cell and the ECM and which plays a critical role in cell spreading and migration [54, 55]. The focal adhesion serves as a bridge between the extracellular substrate and the cell, connecting the extracellular substrate at one end and actin stress fibers at the other, as shown schematically in Figure 6(a). Both the focal adhesion and actin stress fibers are indicators of how strongly a cell binds to the substrate [56-58] and we therefore interrogate the morphology of these two cellular components. To characterize the morphology of actin stress fibers, we stain the cells with fluorescent phalloidin. For cells on hydrogels with smaller meshes, more actin stress fibers are formed, as shown by the red fluorescent stain in Figure 6(b). To investigate the focal adhesion of cells, we immunofluorescently label vinculin, one key structural protein of the focal adhesion [59-61], and quantify the morphology of focal adhesions with confocal microscopy. For all hydrogels, the focal adhesions display elongated shapes at the ends of the stress fibers, with a typical length of 3-5 μm, as shown by the green fluorescent stain in Figure 6(b). The morphology of these focal adhesions suggests that they are in the mature state, since unmatured focal adhesions typically exhibit dot-like structures with lengths less than a micron [62, 63]. The area of single focal adhesions increases as the hydrogel mesh size decreases, as shown in Figure 6(c). Similarly, the number of focal adhesions per cell also increases, as shown in Figure 6(d). As a consequence, the total focal adhesion area per cell increases dramatically as the hydrogel mesh size decreases, as shown in Figure S8. Overall, our results suggest that the ability of cells to form focal adhesion is greatly promoted, and therefore a cell has better adhesion on hydrogels with smaller meshes, as evidenced by the increase of both the number and area of focal adhesion per cell. This also suggests that cells on hydrogels with smaller mesh sizes pull a larger amount of protein, given that the density of the collagen coating is similar among all substrates.

Interestingly, we find a close correlation between focal adhesion area and cell spreading area: cells with larger focal adhesions also tend to have larger spreading areas. This finding agrees with those found for cells on substrates with different stiffnesses [64], despite the fact that the variation here is the hydrogel mesh size rather than the stiffness. However, we observe a positive correlation between focal adhesion size and cell migration speed, which contradicts the biphasic correlation reported previously [65-68]. This likely indicates the focal adhesion size in our study is below the size threshold that inhibits cell migration and therefore positively correlates with cell migration speed.

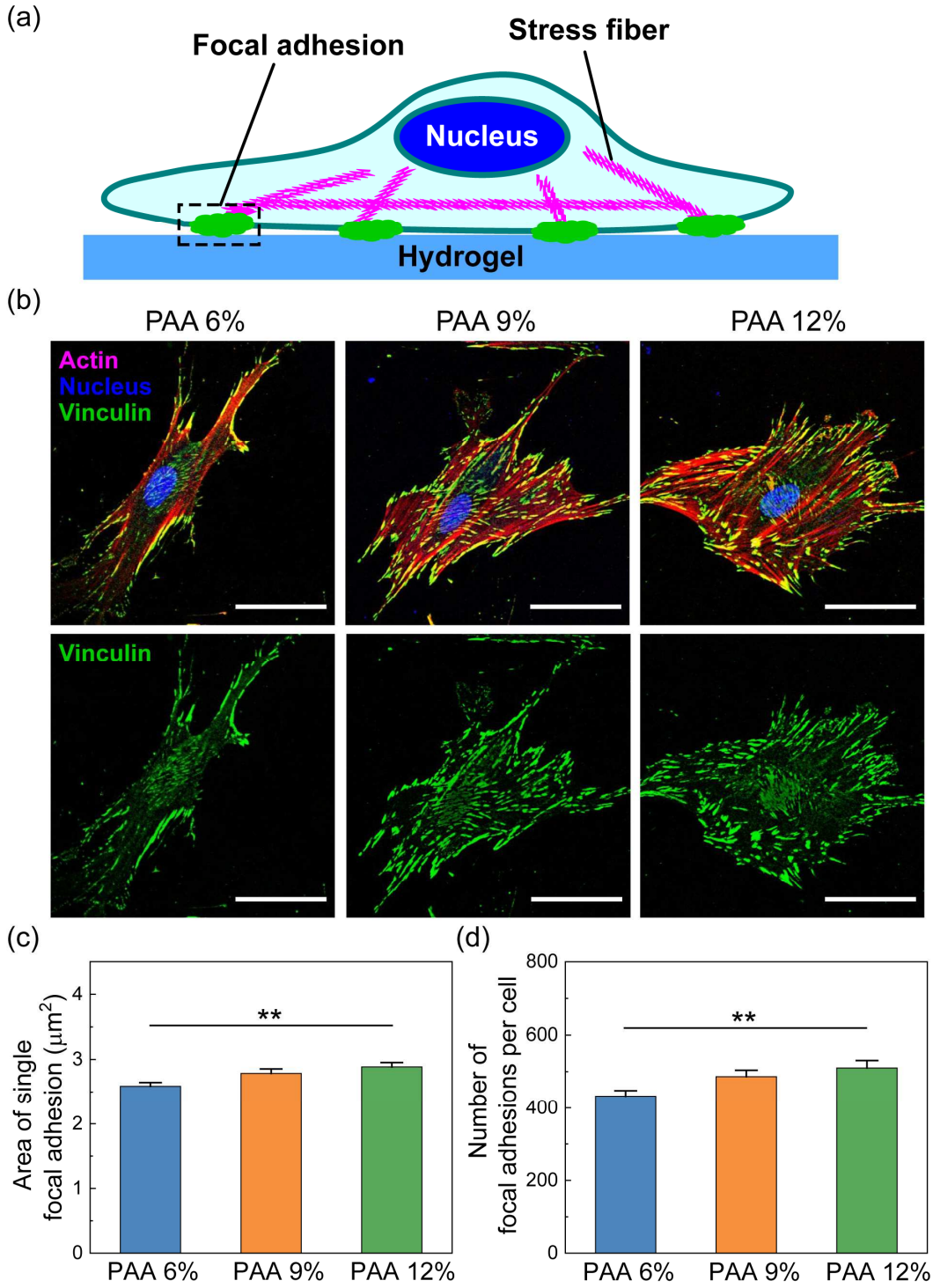

Figure 6. Focal adhesions of cells on hydrogels with different mesh sizes. (a) Schematic of a spreading cell on the hydrogel substrate. The cell adheres to the hydrogel by forming focal adhesions, which are connected to actin stress fibers in the cell. (b) Representative confocal images of stress fibers and focal adhesions of cells on hydrogels with different mesh sizes. Actin is depicted in red; the nucleus is depicted in blue; and vinculin is depicted in green. Scale bars,

50 μm. (c) Area of single focal adhesion of cells on hydrogels with different mesh sizes (Mean ± SE, N>88 per group, one-way ANOVA, $p<0.01$). (d) Number of focal adhesions per cell on hydrogels with different mesh sizes (Mean ± SE, N>88 per group, one-way ANOVA, $p<0.01$).

3.7. Effect of hydrogel mesh size on the yes-associated protein (YAP) nuclear translocation

The key mechanism that regulates cell response to structural and mechanical cues is mechanotransduction [55, 69]. To test whether that is the case for the measurements presented here, we quantify the distribution of yes-associated protein (YAP), a key transcriptional regulator which affects the mechanotransduction of cells by translocating from the cytoplasm to the nucleus [70-74]. The translocation of YAP is regulated by the tension of the F-actin cytoskeleton, which is usually correlated with the formation of stress fibers [75, 76], as illustrated in Figure 7(a). Therefore, we investigate actin and YAP in the cells with immunofluorescent staining and image them with confocal microscopy. As the mesh size of the hydrogel decreases, more stress fibers are formed in cells, as shown in Figure 7(b). In addition, YAP becomes more localized in the nuclear region than the cytosolic region of the cell, as shown in Figure 7(c). We quantify the total fluorescence intensity of YAP in the nucleus and cytosol of cells with ImageJ. The ratio of nuclear to cytosolic YAP increases for the cells grown on hydrogels with smaller meshes, as shown in Figure 7(d). Our results suggest that the mesh size of the hydrogel alters YAP nuclear translocation and acts as a physical regulator that modulates cellular mechanotransduction.

When grown on stiffer substrates, cells have more YAP localized in the nucleus than in the cytoplasm [71, 74]. They also show the enhanced formation of focal adhesions and stress fibers [73, 77]. A possible explanation is that the increased tension exerted through focal adhesions by actomyosin stress fibers opens the nuclear pores and thus allows the entry of YAP from the cytoplasm to the nucleus [76]. Interestingly, similar phenomena are also observed in our systems, suggesting that a similar mechanism of mechanotransduction is triggered by hydrogel mesh size.

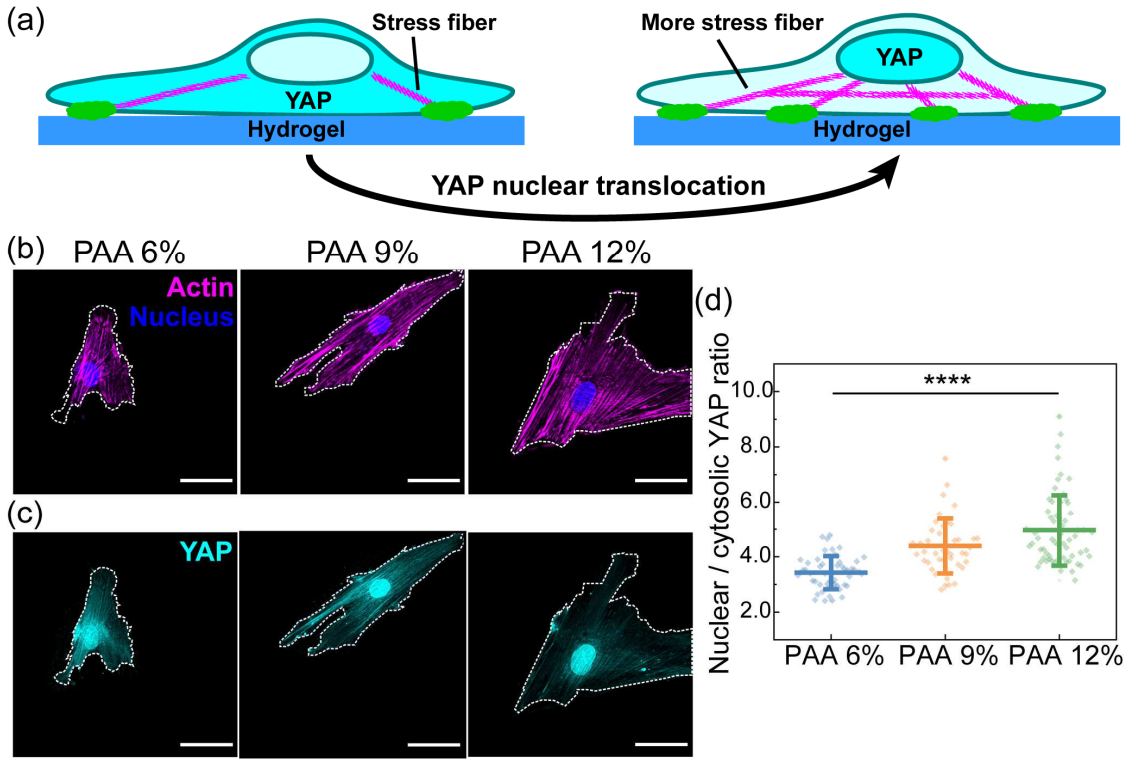

Figure 7. YAP nuclear translocation of cells on hydrogels with different mesh sizes. (a) Schematic view of YAP nuclear translocation. As more stress fibers form in cells, YAP translocates from the cytoplasm to the nucleus of the cell. (b) Representative confocal fluorescence microscopy images of actin stress fibers in cells on hydrogels with different mesh sizes. The outline of the cell is represented by the white dashed line. Actin stress fibers are depicted in red; the nucleus is depicted in blue. Scale bars, 50 μm. (c) Representative confocal fluorescence microscopy images of YAP in cells on hydrogels with different mesh sizes. The outline of the cell is represented by the white dashed line. YAP is depicted in cyan. Scale bars, 50 μm. (d) The ratio of nuclear to cytosolic YAP for cells on hydrogels with different mesh sizes (Mean ± SD, N>42 per group, one-way ANOVA, p<0.0001).

4. Conclusion

In this study, we report a hydrogel system with independently tunable mesh size and stiffness, and use it to isolate the effect of hydrogel mesh size on the behavior of hBMSCs, including cell attachment, spreading, and migration. We show that varying the hydrogel mesh size affects a multitude of cell behavior: the spreading area, nuclear projected area, and migration speed of cells all increase significantly as the mesh size of the hydrogel decreases, while the cell attachment is not affected. At the subcellular scale, both the area and the number of focal adhesions increase as the mesh size of the hydrogel decreases. Furthermore, we find a striking increase in YAP nuclear translocation in cells on hydrogels with smaller meshes, indicating that cellular mechanotransduction is markedly modulated by the mesh size of the hydrogel.

In summary, our study shows that cells respond to the mesh size of hydrogel which is often overlooked in the studies of the cell-substrate interaction, and highlights the important role of mesh size as a structural cue in regulating cell behavior.

This study not only fills in a gap in knowledge in mechanobiology but also provides new insights to use the mesh size as a parameter to regulate cell behavior. Moreover, the results may help in optimizing the structural design of biomaterials in tissue engineering applications. Additionally, this work may deepen our understanding of the mechanics-dependent coordination of physiological and pathological tissue growth. In addition, our results may also be applicable for other fibroblasts, as they share similar phenotypic characteristics and similar responses in short-term assays to mechanical cues [78-81]. Finally, the fundamental mechanisms by which the mesh size affects the cell behavior remain unclear. Possible mechanisms include its influence on nutrient waste diffusion [82] and the variations in the viscous properties of the hydrogel with microstructure [83, 84]. It would be valuable to further explore the complete biological pathway related to hydrogel mesh size in the future.

Acknowledgements

J.X., Z.Y.H., Y.Y. and D.A.W. acknowledge the financial support from the National Science Foundation of United States (DMR-1708729), the National Science Foundation through the Harvard University MRSEC of United States (DMR-2011754, DMR-1420570), and the National Institutes of Health of United States (EB023287). Z.Y.L., Y.S. and X. Q.F. acknowledge the financial support from the National Natural Science Foundation of China (Nos. 11620101001, 11921002 and 042014002).

References

[1] R.O. Hynes, A. Naba, Overview of the matrisome—an inventory of extracellular matrix constituents and functions, Cold Spring Harbor Perspectives in Biology 4(1) (2012) a004903.

[2] T. Yeung, P.C. Georges, L.A. Flanagan, B. Marg, M. Ortiz, M. Funaki, N. Zahir, W.Y. Ming, V. Weaver, P.A. Janmey, Effects of substrate stiffness on cell morphology, cytoskeletal structure, and adhesion, Cell Motil Cytoskel 60(1) (2005) 24-34.

[3] S.R. Caliari, J.A. Burdick, A practical guide to hydrogels for cell culture, Nat Methods 13(5) (2016) 405-14.

[4] M.W. Tibbitt, K.S. Anseth, Hydrogels as Extracellular Matrix Mimics for 3D Cell Culture, Biotechnol Bioeng 103(4) (2009) 655-663.

[5] Y. Li, E. Kumacheva, Hydrogel microenvironments for cancer spheroid growth and drug screening, Sci Adv 4(4) (2018) eaas8998.

[6] A.J. Engler, S. Sen, H.L. Sweeney, D.E. Discher, Matrix elasticity directs stem cell lineage specification, Cell 126(4) (2006) 677-89.

[7] J. Li, D. Han, Y.P. Zhao, Kinetic behaviour of the cells touching substrate: the interfacial stiffness guides cell spreading, Sci Rep 4 (2014) 3910.

[8] J.S. Park, J.S. Chu, A.D. Tsou, R. Diop, Z. Tang, A. Wang, S. Li, The effect of matrix stiffness on the differentiation of mesenchymal stem cells in response to TGF-beta, Biomaterials 32(16) (2011) 3921-30.

[9] L.E. Dickinson, D.R. Rand, J. Tsao, W. Eberle, S. Gerecht, Endothelial cell responses to micropillar substrates of varying dimensions and stiffness, J Biomed Mater Res A 100(6) (2012)

630 1457-66.

631 [10] K. Metavarayuth, P. Sitasuwan, X. Zhao, Y. Lin, Q. Wang, Influence of Surface Topographical
632 Cues on the Differentiation of Mesenchymal Stem Cells in Vitro, Acs Biomaterials Science &
633 Engineering 2(2) (2016) 142-151.

634 [11] M. Akhmanova, E. Osidak, S. Domogatsky, S. Rodin, A. Domogatskaya, Physical, Spatial,
635 and Molecular Aspects of Extracellular Matrix of In Vivo Niches and Artificial Scaffolds Relevant to
636 Stem Cells Research, Stem Cells Int (2015).

637 [12] B. Trappmann, J.E. Gautrot, J.T. Connelly, D.G. Strange, Y. Li, M.L. Oyen, M.A. Cohen Stuart,
638 H. Boehm, B. Li, V. Vogel, J.P. Spatz, F.M. Watt, W.T. Huck, Extracellular-matrix tethering
639 regulates stem-cell fate, Nat Mater 11(7) (2012) 642-9.

640 [13] J.H. Wen, L.G. Vincent, A. Fuhrmann, Y.S. Choi, K.C. Hribar, H. Taylor-Weiner, S. Chen, A.J.
641 Engler, Interplay of matrix stiffness and protein tethering in stem cell differentiation, Nat Mater
642 13(10) (2014) 979-87.

643 [14] M. Rubinstein, R.H. Colby, Polymer physics, Oxford university press New York2003.

644 [15] B.V. Slaughter, S.S. Khurshid, O.Z. Fisher, A. Khademhosseini, N.A. Peppas, Hydrogels in
645 regenerative medicine, Adv Mater 21(32-33) (2009) 3307-29.

646 [16] M.C. LaPlaca, V.N. Vernekar, J.T. Shoemaker, D.K. Cullen, Three-dimensional neuronal
647 cultures, Methods in bioengineering: 3D tissue engineering (2010) 187-204.

648 [17] E.R. Aurand, K.J. Lampe, K.B. Bjugstad, Defining and designing polymers and hydrogels for
649 neural tissue engineering, Neurosci. Res. 72(3) (2012) 199-213.

650 [18] U. Horzum, B. Ozdil, D. Pesen-Okvur, Step-by-step quantitative analysis of focal adhesions,
651 MethodsX 1 (2014) 56-9.

652 [19] J.H. McDonald, Handbook of biological statistics, sparky house publishing Baltimore,
653 MD2009.

654 [20] N.C. Stellwagen, E. Stellwagen, Effect of the matrix on DNA electrophoretic mobility, J
655 Chromatogr A 1216(10) (2009) 1917-1929.

656 [21] N.C. Stellwagen, Effect of the Electric-Field on the Apparent Mobility of Large DNA
657 Fragments in Agarose Gels, Biopolymers 24(12) (1985) 2243-2255.

658 [22] A.G. Ogston, The Spaces in a Uniform Random Suspension of Fibres, T Faraday Soc 54(11)
659 (1958) 1754-1757.

660 [23] M. Galli, M. Oyen, Spherical indentation of a finite poroelastic coating, Appl Phys Lett 93(3)
661 (2008) 031911.

662 [24] A. Buxboim, K. Rajagopal, A.E. Brown, D.E. Discher, How deeply cells feel: methods for thin
663 gels, J Phys Condens Matter 22(19) (2010) 194116.

664 [25] E.K. Dimitriadis, F. Horkay, J. Maresca, B. Kachar, R.S. Chadwick, Determination of elastic
665 moduli of thin layers of soft material using the atomic force microscope, Biophys. J. 82(5) (2002)
666 2798-2810.

667 [26] A.A. Khalili, M.R. Ahmad, A Review of Cell Adhesion Studies for Biomedical and Biological
668 Applications, Int. J. Mol. Sci. 16(8) (2015) 18149-18184.

669 [27] J.P. Stegemann, H. Hong, R.M. Nerem, Mechanical, biochemical, and extracellular matrix
670 effects on vascular smooth muscle cell phenotype, J Appl Physiol (1985) 98(6) (2005) 2321-7.

671 [28] Y. Artemenko, L. Axiotakis, Jr., J. Borleis, P.A. Iglesias, P.N. Devreotes, Chemical and
672 mechanical stimuli act on common signal transduction and cytoskeletal networks, Proc Natl Acad
673 Sci U S A 113(47) (2016) E7500-E7509.

[29] C. Gaudet, W.A. Marganski, S. Kim, C.T. Brown, V. Gunderia, M. Dembo, J.Y. Wong, Influence of type I collagen surface density on fibroblast spreading, motility, and contractility, Biophysical Journal 85(5) (2003) 3329-3335.

[30] A. Engler, L. Bacakova, C. Newman, A. Hategan, M. Griffin, D. Discher, Substrate compliance versus ligand density in cell on gel responses, Biophysical Journal 86(1) (2004) 617-628.

[31] A.J. Engler, L. Richert, J.Y. Wong, C. Picart, D.E. Discher, Surface probe measurements of the elasticity of sectioned tissue, thin gels and polyelectrolyte multilayer films: Correlations between substrate stiffness and cell adhesion, Surf Sci 570(1-2) (2004) 142-154.

[32] J.P. Orgel, A. Miller, T.C. Irving, R.F. Fischetti, A.P. Hammersley, T.J. Wess, The in situ supermolecular structure of type I collagen, Structure 9(11) (2001) 1061-9.

[33] M. Gale, M.S. Pollanen, P. Markiewicz, M.C. Goh, Sequential assembly of collagen revealed by atomic force microscopy, Biophys J 68(5) (1995) 2124-8.

[34] J.K. Mouw, G. Ou, V.M. Weaver, Extracellular matrix assembly: a multiscale deconstruction, Nat Rev Mol Cell Biol 15(12) (2014) 771-85.

[35] J.P. Lee, E. Kassianidou, J.I. MacDonald, M.B. Francis, S. Kumar, N-terminal specific conjugation of extracellular matrix proteins to 2-pyridinecarboxaldehyde functionalized polyacrylamide hydrogels, Biomaterials 102 (2016) 268-76.

[36] T. Gurry, P.S. Nerenberg, C.M. Stultz, The contribution of interchain salt bridges to triple-helical stability in collagen, Biophys J 98(11) (2010) 2634-43.

[37] W.J. Hadden, J.L. Young, A.W. Holle, M.L. McFetridge, D.Y. Kim, P. Wijesinghe, H. Taylor-Weiner, J.H. Wen, A.R. Lee, K. Bieback, Stem cell migration and mechanotransduction on linear stiffness gradient hydrogels, Proceedings of the National Academy of Sciences 114(22) (2017) 5647-5652.

[38] B.C. Isenberg, P.A. Dimilla, M. Walker, S. Kim, J.Y. Wong, Vascular smooth muscle cell durotaxis depends on substrate stiffness gradient strength, Biophys J 97(5) (2009) 1313-22.

[39] A.E. Stanton, X. Tong, F. Yang, Varying solvent type modulates collagen coating and stem cell mechanotransduction on hydrogel substrates, APL Bioeng 3(3) (2019) 036108.

[40] J.L. McGrath, Cell spreading: the power to simplify, Curr. Biol. 17(10) (2007) R357-8.

[41] J. Folkman, A. Moscona, Role of cell shape in growth control, Nature 273(5661) (1978) 345-9.

[42] C.S. Chen, M. Mrksich, S. Huang, G.M. Whitesides, D.E. Ingber, Geometric control of cell life and death, Science 276(5317) (1997) 1425-8.

[43] M. Guo, A.F. Pegoraro, A. Mao, E.H. Zhou, P.R. Arany, Y. Han, D.T. Burnette, M.H. Jensen, K.E. Kasza, J.R. Moore, F.C. Mackintosh, J.J. Fredberg, D.J. Mooney, J. Lippincott-Schwartz, D.A. Weitz, Cell volume change through water efflux impacts cell stiffness and stem cell fate, Proc Natl Acad Sci USA 114(41) (2017) E8618-E8627.

[44] R. Vishavkarma, S. Raghavan, C. Kuyyamudi, A. Majumder, J. Dhawan, P.A. Pullarkat, Role of actin filaments in correlating nuclear shape and cell spreading, PLoS One 9(9) (2014) e107895.

[45] J. Xia, Y. Yuan, H. Wu, Y. Huang, D.A. Weitz, Decoupling the effects of nanopore size and surface roughness on the attachment, spreading and differentiation of bone marrow-derived stem cells, Biomaterials 248 (2020) 120014.

[46] K. Webb, V. Hlady, P.A. Tresco, Relationships among cell attachment, spreading, cytoskeletal organization, and migration rate for anchorage-dependent cells on model surfaces, J Biomed Mater Res 49(3) (2000) 362-368.

[47] D.A. Lauffenburger, A.F. Horwitz, Cell migration: a physically integrated molecular process,

719 Cell 84(3) (1996) 359-69.

720 [48] A.J. Ridley, M.A. Schwartz, K. Burridge, R.A. Firtel, M.H. Ginsberg, G. Borisy, J.T. Parsons,
721 A.R. Horwitz, Cell migration: integrating signals from front to back, Science 302(5651) (2003)
722 1704-9.

723 [49] D.R. Nisbet, J.S. Forsythe, W. Shen, D.I. Finkelstein, M.K. Horne, Review paper: a review of
724 the cellular response on electrospun nanofibers for tissue engineering, J Biomater Appl 24(1)
725 (2009) 7-29.

726 [50] K. Kolind, K.W. Leong, F. Besenbacher, M. Foss, Guidance of stem cell fate on 2D patterned
727 surfaces, Biomaterials 33(28) (2012) 6626-33.

728 [51] J. Wang, J.W. Petefish, A.C. Hillier, I.C. Schneider, Epitaxially grown collagen fibrils reveal
729 diversity in contact guidance behavior among cancer cells, Langmuir 31(1) (2015) 307-14.

730 [52] B.D. Harms, G.M. Bassi, A.R. Horwitz, D.A. Lauffenburger, Directional persistence of EGF-
731 induced cell migration is associated with stabilization of lamellipodial protrusions, Biophys J 88(2)
732 (2005) 1479-88.

733 [53] M. Krause, A. Gautreau, Steering cell migration: lamellipodium dynamics and the regulation
734 of directional persistence, Nat Rev Mol Cell Biol 15(9) (2014) 577-90.

735 [54] D.E. Discher, P. Janmey, Y.L. Wang, Tissue cells feel and respond to the stiffness of their
736 substrate, Science 310(5751) (2005) 1139-1143.

737 [55] D.E. Jaalouk, J. Lammerding, Mechanotransduction gone awry, Nat Rev Mol Cell Biol 10(1)
738 (2009) 63-73.

739 [56] S. Tojkander, G. Gateva, P. Lappalainen, Actin stress fibers--assembly, dynamics and
740 biological roles, J Cell Sci 125(Pt 8) (2012) 1855-64.

741 [57] N.D. Gallant, K.E. Michael, A.J. Garcia, Cell adhesion strengthening: contributions of
742 adhesive area, integrin binding, and focal adhesion assembly, Mol Biol Cell 16(9) (2005) 4329-40.

743 [58] K.E. Michael, A.J. García, Cell Adhesion Strengthening: Measurement and Analysis, Cell
744 Mechanics2007, pp. 329-346.

745 [59] K. Haase, Z. Al-Rekabi, A.E. Pelling, Mechanical cues direct focal adhesion dynamics, Prog
746 Mol Biol Transl Sci 126 (2014) 103-34.

747 [60] K. Hayakawa, H. Tatsumi, M. Sokabe, Mechano-sensing by actin filaments and focal
748 adhesion proteins, Communicative & Integrative Biology 5(6) (2012) 572-577.

749 [61] G.R. Owen, D. Meredith, R. Richards, Focal adhesion quantification-a new assay of material
750 biocompatibility? Review, Eur Cells Mater 9 (2005) 85-96; discussion 85-96.

751 [62] M.A. Partridge, E.E. Marcantonio, Initiation of attachment and generation of mature focal
752 adhesions by integrin-containing filopodia in cell spreading, Mol Biol Cell 17(10) (2006) 4237-48.

753 [63] C.W. Kuo, D.Y. Chueh, P. Chen, Investigation of size-dependent cell adhesion on
754 nanostructured interfaces, J Nanobiotechnology 12 (2014) 54.

755 [64] D.-H. Kim, D. Wirtz, Predicting how cells spread and migrate: focal adhesion size does
756 matter, Cell Adhesion & Migration 7(3) (2013) 293-296.

757 [65] D.H. Kim, D. Wirtz, Focal adhesion size uniquely predicts cell migration, Faseb J 27(4) (2013)
758 1351-1361.

759 [66] S.P. Palecek, J.C. Loftus, M.H. Ginsberg, D.A. Lauffenburger, A.F. Horwitz, Integrin-ligand
760 binding properties govern cell migration speed through cell-substratum adhesiveness, Nature
761 385(6616) (1997) 537-540.

762 [67] G. Maheshwari, G. Brown, D.A. Lauffenburger, A. Wells, L.G. Griffith, Cell adhesion and

motility depend on nanoscale RGD clustering, J Cell Sci 113(10) (2000) 1677-1686.

[68] P.A. DiMilla, K. Barbee, D.A. Lauffenburger, Mathematical model for the effects of adhesion and mechanics on cell migration speed, Biophysical Journal 60(1) (1991) 15-37.

[69] Y. Sun, C.S. Chen, J. Fu, Forcing stem cells to behave: a biophysical perspective of the cellular microenvironment, Annu Rev Biophys 41 (2012) 519-42.

[70] A. Totaro, T. Panciera, S. Piccolo, YAP/TAZ upstream signals and downstream responses, Nat Cell Biol 20(8) (2018) 888-899.

[71] S. Dupont, Role of YAP/TAZ in cell-matrix adhesion-mediated signalling and mechanotransduction, Exp Cell Res 343(1) (2016) 42-53.

[72] S.E. Hiemer, A.D. Szymaniak, X. Varelas, The transcriptional regulators TAZ and YAP direct transforming growth factor beta-induced tumorigenic phenotypes in breast cancer cells, J Biol Chem 289(19) (2014) 13461-74.

[73] G. Nardone, J. Oliver-De La Cruz, J. Vrbsky, C. Martini, J. Pribyl, P. Skladal, M. Pesl, G. Caluori, S. Pagliari, F. Martino, Z. Maceckova, M. Hajduch, A. Sanz-Garcia, N.M. Pugno, G.B. Stokin, G. Forte, YAP regulates cell mechanics by controlling focal adhesion assembly, Nat Commun 8 (2017) 15321.

[74] S. Dupont, L. Morsut, M. Aragona, E. Enzo, S. Giulitti, M. Cordenonsi, F. Zanconato, J. Le Digabel, M. Forcato, S. Bicciato, N. Elvassore, S. Piccolo, Role of YAP/TAZ in mechanotransduction, Nature 474(7350) (2011) 179-83.

[75] K. Wada, K. Itoga, T. Okano, S. Yonemura, H. Sasaki, Hippo pathway regulation by cell morphology and stress fibers, Development 138(18) (2011) 3907-14.

[76] A. Elosegui-Artola, I. Andreu, A.E.M. Beedle, A. Lezamiz, M. Uroz, A.J. Kosmalska, R. Oria, J.Z. Kechagia, P. Rico-Lastres, A.L. Le Roux, C.M. Shanahan, X. Trepat, D. Navajas, S. Garcia-Manyes, P. Roca-Cusachs, Force Triggers YAP Nuclear Entry by Regulating Transport across Nuclear Pores, Cell 171(6) (2017) 1397-1410 e14.

[77] S. Fusco, V. Panzetta, P.A. Netti, Mechanosensing of substrate stiffness regulates focal adhesions dynamics in cell, Meccanica 52(14) (2017) 3389-3398.

[78] B. Venugopal, P. Mogha, J. Dhawan, A. Majumder, Cell density overrides the effect of substrate stiffness on human mesenchymal stem cells' morphology and proliferation, Biomaterials Science 6(5) (2018) 1109-1119.

[79] A. Chopra, M.E. Murray, F.J. Byfield, M.G. Mendez, R. Halleluyan, D.J. Restle, D.R.-B. Aroush, P.A. Galie, K. Pogoda, R. Bucki, Augmentation of integrin-mediated mechanotransduction by hyaluronic acid, Biomaterials 35(1) (2014) 71-82.

[80] M. Guo, A.F. Pegoraro, A. Mao, E.H. Zhou, P.R. Arany, Y. Han, D.T. Burnette, M.H. Jensen, K.E. Kasza, J.R. Moore, Cell volume change through water efflux impacts cell stiffness and stem cell fate, Proceedings of the National Academy of Sciences 114(41) (2017) E8618-E8627.

[81] R.A. Denu, S. Nemcek, D.D. Bloom, A.D. Goodrich, J. Kim, D.F. Mosher, P. Hematti, Fibroblasts and Mesenchymal Stromal/Stem Cells Are Phenotypically Indistinguishable, Acta Haematol 136(2) (2016) 85-97.

[82] H. Yu, I. Meyvantsson, I.A. Shkel, D.J. Beebe, Diffusion dependent cell behavior in microenvironments, Lab Chip 5(10) (2005) 1089-95.

[83] J.M. Grolman, P. Weinand, D.J. Mooney, Extracellular matrix plasticity as a driver of cell spreading, Proceedings of the National Academy of Sciences 117(42) (2020) 25999-26007.

[84] O. Chaudhuri, L. Gu, D. Klumpers, M. Darnell, S.A. Bencherif, J.C. Weaver, N. Huebsch, H.P. Lee, E. Lippens, G.N. Duda, D.J. Mooney, Hydrogels with tunable stress relaxation regulate stem

808 cell fate and activity, Nat Mater 15(3) (2016) 326-34.
809

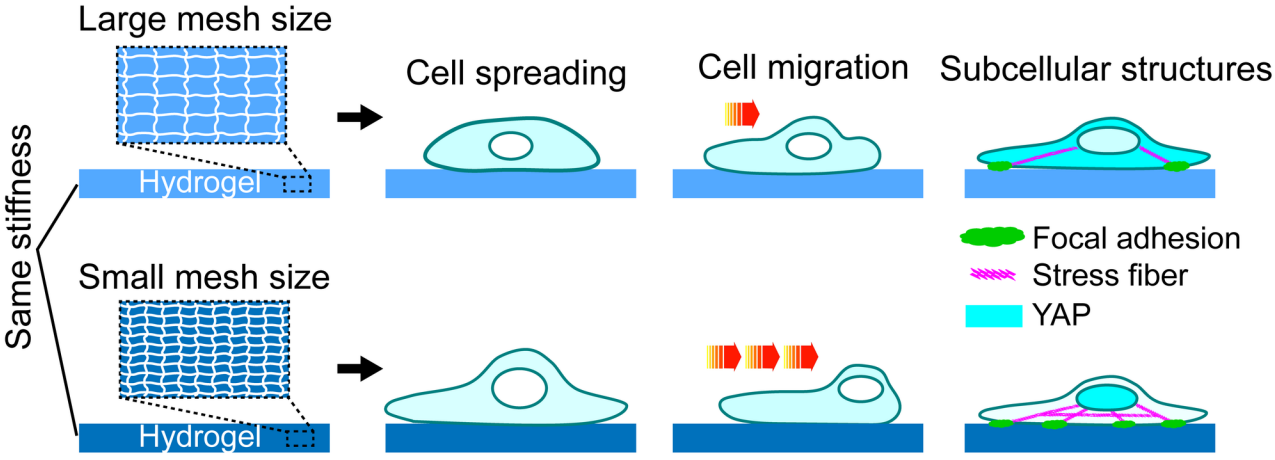
Large mesh size
Cell spreading
Cell migration
Subcellular structures
Same stiffness
Hydrogel
Focal adhesion
Stress fiber
YAP
Small mesh size
Hydrogel